

**$^{12}\text{C}$ -induced single particle transfer reactions at  $E/A = 50$  MeV**

J. S. Winfield, E. Adamides,\* Sam M. Austin, G. M. Crawley, M. F. Mohar, C. A. Ogilvie,  
B. Sherrill, M. Torres,<sup>†</sup> and G. Yoo

*National Superconducting Cyclotron Laboratory and Department of Physics and Astronomy, Michigan State University,  
East Lansing, Michigan 48824*

A. Nadasen<sup>‡</sup>

*Department of Natural Sciences, University of Michigan, Dearborn, Michigan 48128*

(Received 21 November 1988)

Differential cross-section angular distributions have been measured for single-nucleon transfer reactions induced by  $E/A = 50$  MeV  $^{12}\text{C}$  on targets of  $^{12}\text{C}$ ,  $^{27}\text{Al}$ ,  $^{40}\text{Ca}$ ,  $^{90}\text{Zr}$ , and  $^{208}\text{Pb}$ . Finite-range distorted-wave Born-approximation calculations reproduce the shape of the angular distributions for all targets. Although the cross-section magnitudes are sensitive to the choice of distorting potentials, reasonable potentials are found that yield spectroscopic factors within 50% of light-ion results for all targets.

**I. INTRODUCTION**

The distorted-wave Born approximation (DWBA) has been extensively used to describe low-energy single-nucleon transfer reactions. At energies well above  $E/A = 10$  MeV, however, individual nucleon-nucleon interactions are expected to become more important than nucleon-nucleus interactions,<sup>1</sup> which may invalidate the mean-field assumptions inherent in the DWBA. Such a breakdown of the DWBA might be manifested by an apparent need for an energy dependence of the effective nucleon-nucleus interaction, although the use of phenomenological optical-model potentials (OMP's) might obscure any effect on the cross sections.

A study<sup>2</sup> of the  $^{208}\text{Pb}(^{16}\text{O},^{15}\text{N})^{209}\text{Bi}$  and  $^{208}\text{Pb}(^{16}\text{O},^{15}\text{O})^{209}\text{Pb}$  reactions at  $E/A = 50$  MeV found that the DWBA overpredicted the data by a factor of about 10. This discrepancy by far exceeds anomalies found in DWBA analyses of transfer reactions at or below  $E/A = 10$  MeV that have often been attributed to coupled-channel effects or to uncertainties in the bound-state description, etc. Furthermore, it is not an isolated result: For the same  $^{16}\text{O} + ^{208}\text{Pb}$  system, Olmer *et al.*<sup>3</sup> had previously noted a trend for DWBA to overpredict cross sections as the bombarding energy was increased from  $E/A = 6.5$  to 20 MeV. At  $E/A = 20$  MeV, the ratio  $R = \sigma(\text{DWBA})/\sigma(\text{expt})$  ranged from 2 to 3, depending on the particular final state involved.

Other intermediate energy heavy-ion transfer reactions add little support to an energy dependence of  $R$ . For example, Fernandes *et al.*<sup>4</sup> studied transfer reactions induced by  $E/A = 20$ -MeV  $^{18}\text{O}$  projectiles on a  $^{28}\text{Si}$  target and were able to reproduce the cross sections with DWBA calculations that used deep real Wood-Saxon potentials to generate the distorted waves, although surface-transparent potentials with very shallow real strengths overpredicted the data by a factor of about 3. Transfer reactions induced by  $^{13}\text{C}$  projectiles have been studied at  $E/A = 30$  MeV on a quite extensive range of

targets ( $^{12}\text{C}$ ,  $^{27}\text{Al}$ ,  $^{58}\text{Ni}$ , and  $^{90}\text{Zr}$ ) by von Oertzen *et al.*,<sup>5</sup> and DWBA calculations have given satisfactory agreement for the cross sections. In addition, the same group that found the large discrepancy in  $^{16}\text{O} + ^{208}\text{Pb}$  have reported that DWBA calculations do reproduce data for one-nucleon-stripping reactions induced by  $E/A = 40$  MeV  $^{12}\text{C}$  on a  $^{208}\text{Pb}$  target.<sup>6</sup>

To help understand these apparent inconsistencies, we have undertaken a systematic study of single-nucleon transfer reactions induced by  $E/A = 50$ -MeV  $^{12}\text{C}$  on a wide mass range of targets. The reactions studied were  $^{12}\text{C}(^{12}\text{C}, ^{13}\text{C})^{11}\text{C}$ ,  $^{27}\text{Al}(^{12}\text{C}, ^{11}\text{B})^{28}\text{Si}$ ,  $^{40}\text{Ca}(^{12}\text{C}, ^{11}\text{C})^{41}\text{Ca}$ ,  $^{90}\text{Zr}(^{12}\text{C}, ^{13}\text{N})^{89}\text{Y}$ , and  $^{208}\text{Pb}(^{12}\text{C}, ^{11}\text{B})^{208}\text{Bi}$ . The  $^{12}\text{C}$  target data have been published in preliminary form in Ref. 7.

In the past, studies of heavy-ion transfer reactions have been plagued by uncertainties arising from ambiguities in the optical-model potential. The strong absorption in heavy-ion elastic scattering has restricted its sensitivity to the extreme surface region of the nucleus, and a variety of potentials can provide fits to the data, provided that they have similar values in this critical region. However, for higher bombarding energies, the potential is probed over a wider domain inside the strong absorption radius,<sup>8</sup> and there is evidence<sup>9,10</sup> that phenomenological optical-model potentials can be quite precisely determined, at least for relatively light projectiles and targets. In the present work, we find that potentials with the same characteristics (shallow imaginary wells) as determined<sup>9</sup> by high-energy  $^{12}\text{C} + ^{12}\text{C}$  and  $^{16}\text{O} + ^{12}\text{C}$  elastic scattering measured over a large angular range, perform best in the DWBA transfer predictions for the  $^{12}\text{C}$  and  $^{27}\text{Al}$  targets. Unfortunately, detailed elastic scattering data is not available for  $A_{\text{proj}} > 6$  on heavy targets. In any case, we find that the sensitivity to the choice of optical-model potential would not obscure an anomaly as strong as that seen<sup>2</sup> in the  $^{16}\text{O} + ^{208}\text{Pb}$  transfer reactions.

Following a description of the experimental procedure in Sec. II, we discuss the general features of the spectra in

Sec. III. In Sec. IV, the results of finite-range DWBA calculations are presented. In Sec. V the conclusions are drawn.

## II. EXPERIMENTAL PROCEDURE

The experiment was performed with an  $E/A = 50.4$ -MeV  $^{12}\text{C}^{5+}$  beam from the K500 cyclotron at the National Superconducting Cyclotron Laboratory. Beam currents on target ranged from about 2 to 20 particle nA during the reactions runs, and about 0.5 particle nA during the elastic scattering runs. The uncertainty in the beam energy is about  $\pm 2\%$ . The target thicknesses (with isotopic purities given in parentheses) were as follows:  $^{12}\text{C}$  1.05 mg/cm<sup>2</sup> (natural);  $^{27}\text{Al}$  1.25 mg/cm<sup>2</sup>;  $^{40}\text{Ca}$  2.41 mg/cm<sup>2</sup> (natural);  $^{90}\text{Zr}$  1.07 mg/cm<sup>2</sup> (98.7%);  $^{208}\text{Pb}$  3.10 mg/cm<sup>2</sup> (99.9%). All target thicknesses were measured by the  $\alpha$ -particle energy-loss technique to an accuracy of about  $\pm 5\%$ . The  $^{40}\text{Ca}$  and  $^{208}\text{Pb}$  targets were stored and transferred to the target chamber under vacuum.

The reaction products were analyzed by the S-320 spectrograph<sup>11</sup> with a resolution of about 1 MeV. By means of interchangeable sets of aperture slits and holes, the solid angle of acceptance for the reaction runs was set between 0.03 and 0.67 msr ( $\pm 0.19^\circ$  to  $\pm 0.74^\circ$  horizontal angular acceptance, respectively), depending on the reaction yield.

The focal plane detector consisted of two single-wire proportional counters separated by two ionization counters and a thick plastic scintillator that stopped the ions. Adequate particle identification (PI) was obtained through the energy-loss signal from the ion chambers, time of flight relative to the cyclotron rf, and the light output from the scintillator.

A set of four monitor detectors, arranged symmetrically around the beam axis, was used to determine the relative cross sections for different spectrograph angles. These detectors were  $4 \times 4$  mm<sup>2</sup> Hamamatsu PIN photodiodes, fixed at a distance of about 15 cm from the target and at an angle of about  $12.5^\circ$  to the beam. Absolute cross sections were determined by the integrated current from a Faraday cup which was fixed on the beam axis. The efficiency of the Faraday cup was checked by measuring elastic scattering from a gold target at small angles where Rutherford scattering dominates. For the measured gold target thickness, the elastic scattering yield agreed with optical-model predictions to within 5% in the c.m. angular range from  $3.5^\circ$  to  $5^\circ$ . This measurement was repeated throughout the experiment as a check against possible changes in beam position or angle of incidence. The measurements showed changes in the elastic scattering yield by no more than 7% during the course of the experiment. A conservative estimate of the overall systematic uncertainty from all sources is  $\pm 15\%$ .

The focal plane of the spectrometer was calibrated by varying the magnetic elements to step elastically scattered  $^{12}\text{C}$  particles across the region of interest. The calibration points were fitted by a second-order polynomial. In addition, single spectra for  $^{12}\text{C}(^{12}\text{C}, ^{13}\text{N})^{11}\text{B}$  and  $^{27}\text{Al}(^{12}\text{C}, ^{13}\text{N})^{26}\text{Mg}$  were obtained at the same field settings as a sample  $^{90}\text{Zr}(^{12}\text{C}, ^{13}\text{N})^{89}\text{Y}$  reaction measurement;

the resolved low-lying states in  $^{11}\text{B}$  and  $^{26}\text{Mg}$  were then used to fix the calibration for the  $^{89}\text{Y}$  spectrum.

## III. RESULTS

Spectra for all the targets are shown in Figs. 1 and 2. Typically, relatively high-spin states tend to be favored, which reflects the large momentum transfer imparted by these high-energy heavy-ion reactions.<sup>12</sup> We have concentrated on states of the residual nuclei which are known to have strong single-particle character. Except for the  $^{12}\text{C}(^{12}\text{C}, ^{13}\text{C})^{11}\text{C}$  reaction, excitation of the ejectile nucleus is not evident in the spectra (for the  $^{90}\text{Zr}(^{12}\text{C}, ^{13}\text{N})^{89}\text{Y}$  reaction, ejectile excitation would not be observed since  $^{13}\text{N}$  has no bound excited states). Inhibition of multistep processes, such as mutual excitation, might be expected due to the short interaction times at high bombarding energies relative to the Fermi velocities of the participating nucleons.

A discussion of the individual reactions follows.

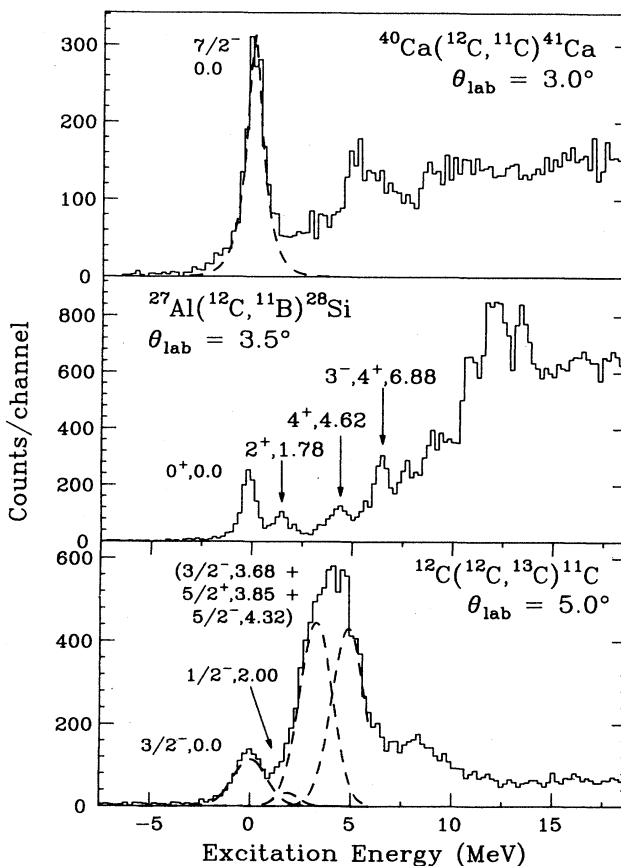


FIG. 1. Spectra of single-nucleon transfer reactions induced by  $E/A = 50$ -MeV  $^{12}\text{C}$  on targets of  $^{12}\text{C}$ ,  $^{27}\text{Al}$ , and  $^{40}\text{Ca}$ . Known low-lying states in the residual nuclei are indicated. The dashed lines in the  $^{12}\text{C}$  and  $^{40}\text{Ca}$  spectra are the results of multiple Gaussian fits described in the text.

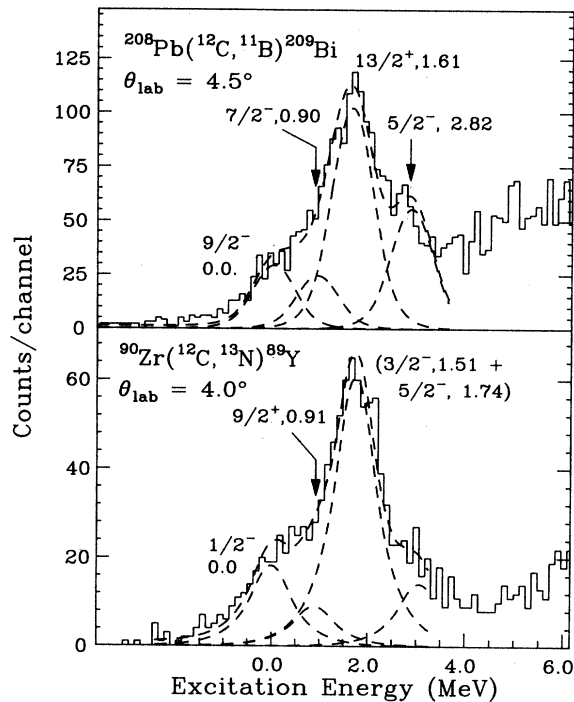


FIG. 2. Spectra of single-nucleon transfer reactions induced by  $E/A = 50$ -MeV  $^{12}\text{C}$  on targets of  $^{90}\text{Zr}$  and  $^{208}\text{Pb}$ . Low-lying states in the residual nuclei are indicated by spin, parity, and excitation energy. The dashed lines are the results of multiple Gaussian fits described in the text.

#### A. $^{12}\text{C}(^{12}\text{C}, ^{13}\text{C})^{11}\text{C}$

The strongest peak observed (Fig. 1) in this neutron-pickup reaction corresponds to the unresolved  $\frac{3}{2}^-$  (3.68 MeV) and  $\frac{5}{2}^+$  (3.85 MeV) states in  $^{13}\text{C}$ , and the  $\frac{5}{2}^-$  (4.32 MeV) state in  $^{11}\text{C}$ ; the ground-state peak of interest is about eight times weaker. The yield to the ground state has been extracted from multiple-Gaussian fits with the separation of the ground and first excited states fixed from the focal plane calibration and two representative peaks used in the 3–5-MeV region. The areas of the unfolded peaks of ground and first excited states compare well with spectra for the same reaction taken at  $E/A = 25$  and 35 MeV,<sup>7</sup> where the low-lying states are better resolved.

#### B. $^{27}\text{Al}(^{12}\text{C}, ^{11}\text{B})^{28}\text{Si}$

The spectrum for this proton-stripping reaction (Fig. 1) appears quite similar in regard to the distribution of yield to the  $(\alpha, t)$  spectrum measured by Ciangaru *et al.*<sup>13</sup> The yield between 11 and 15 MeV is identified in Ref. 13 as excitation of the  $6^-$ ,  $T=0$  (11.58 MeV) state and three  $T=1$  states ( $4^-$ ,  $5^-$ , and  $6^-$ ) that are analogs of levels in  $^{28}\text{Al}$ .

#### C. $^{40}\text{Ca}(^{12}\text{C}, ^{11}\text{C})^{41}\text{Ca}$

Transfer to the  $\frac{7}{2}^-$  ground state dominates this neutron-stripping reaction (Fig. 1). Immediately above

this state lie a number of unresolved levels, of which the strongest are expected<sup>14,15</sup> to be the  $\frac{3}{2}^-$  1.94-MeV,  $\frac{3}{2}^-$  2.46-MeV, and  $\frac{1}{2}^-$  3.94-MeV excited states of  $^{41}\text{Ca}$ . We note that in the  $^{40}\text{Ca}(^{14}\text{C}, ^{13}\text{C})^{41}\text{Ca}$  reaction at 64 MeV (Ref. 14), the ground-state yield is commensurate with that of the 1.94-MeV state. The fact that the ground state (mainly  $0f_{7/2}$ ) dominates in the present ( $^{12}\text{C}, ^{11}\text{C}$ ) data at 600 MeV probably reflects the preference for higher angular momentum transfer as the bombarding energy is increased.<sup>12</sup> To extract the yield for the ground state, a four-fold peak fit was performed; the first peak being the ground state and the others are the three main levels listed above. For clarity, only the unfolded peak fit to the ground state is displayed in Fig. 1.

#### D. $^{90}\text{Zr}(^{12}\text{C}, ^{13}\text{N})^{89}\text{Y}$

The spectrum of this proton-pickup reaction (Fig. 2) is dominated by two peaks, the  $\frac{1}{2}^-$  ground state of  $^{89}\text{Y}$  and a broad peak next to it which consists of low-lying excited states in  $^{89}\text{Y}$ , i.e., the mainly  $0g_{9/2}$ ,  $1p_{3/2}$ ,  $0f_{5/2}$ , and  $1d_{5/2}$  configurations at 0.91, 1.51, 1.74, and 2.22 MeV, respectively. From previously studied proton-pickup reactions on  $^{90}\text{Zr}$ ,  $^{90}\text{Zr}(d, ^3\text{He})$  at 52 MeV (Ref. 16),  $^{90}\text{Zr}(^{13}\text{C}, ^{14}\text{N})$  at  $E/A = 30$  MeV (Ref. 17), and  $^{90}\text{Zr}(^6\text{Li}, ^7\text{Be})$  at  $E/A = 10$  (Ref. 18), one expects the ground state, the 1.51-MeV state, and the 1.75-MeV state to be the most strongly populated.

In the analysis, peaks of Gaussian shape with exponential tails were used. The peak shape was based on that observed in  $^{40}\text{Ca}(^{12}\text{C}, ^{11}\text{C})^{41}\text{Ca}$  where the ground state is well separated. The method of analysis was to specify a sequence of four peaks, the first three of which corresponded to the ground state, and the 0.91- and 1.74-MeV excited state of  $^{89}\text{Y}$  at the known separation energies (tests showed that the fit was very insensitive to the inclusion of the 1.51-MeV state). The remaining peak was used to reproduce the higher excitation region of unresolved states. The positions of the three lower-energy peaks were allowed to move as a group, with widths set equal and fixed, while the  $\chi^2$  was minimized. The areas of the unfolded peaks for the low-lying states compare well with the spectrum obtained<sup>16</sup> for  $^{90}\text{Zr}(d, ^3\text{He})^{89}\text{Y}$ . As a check, several spectra were reanalyzed by a second approach in which the broad peak next to ground state was fitted by two overlapping peaks. The position of all three peaks was set free for the best fit to the data, with widths again held equal and fixed. The two methods gave yields for the ground state which differed by less than 15%.

#### E. $^{208}\text{Pb}(^{12}\text{C}, ^{11}\text{B})^{209}\text{Bi}$

This proton-stripping reaction has been studied recently by Mermaz *et al.*<sup>6</sup> at  $E/A = 40$  MeV. From the better resolution in their spectra, the only states below 3 MeV with observable yield are known<sup>19</sup> states of  $^{209}\text{Bi}$ , i.e., ejectile excitation does not appear to contribute significantly. Based on this, we have analyzed our spectrum (Fig. 2) by specifying a sequence of four peaks corresponding to the first four states in  $^{209}\text{Bi}$  at the known excitation energies. The positions of these four peaks

were allowed to move as a group, with widths set equal and fixed, while the  $\chi^2$  was minimized.

The cross sections that we obtain for the  $^{208}\text{Pb}(^{12}\text{C}, ^{11}\text{B})^{209}\text{Bi}$  reaction at  $E/A = 50$  MeV are almost a factor of 3 lower than those measured at  $E/A = 40$  MeV by Mermaz *et al.*<sup>6</sup> (comparing at equivalent  $q$  transfer), whereas the peak cross section<sup>20</sup> for  $E/A = 6.4, 8.2,$  and  $9.7$  MeV rises monotonically with increasing bombarding energy. It thus appears that there is an energy above  $E/A = 40$  MeV, beyond which the experimental peak cross section turns over and begins to decrease, as might be expected<sup>12</sup> from considerations of the linear momentum transfer necessary and the maximum nucleon velocity available at the Fermi surface. However, DWBA calculations at  $E/A = 40$  and  $50$  MeV with similar optical-model potentials do not reproduce this behavior (compare results for potential PB4 in Sec. IV C).

#### IV. DWBA ANALYSIS

##### A. Computational details

The DWBA analysis was performed with the full-recoil finite-range programs PTOLEMY (Ref. 21) and SATURN-MARS (Ref. 22). Tests showed that in the angular range of the measured data, PTOLEMY predicted cross sections about 40% lower on average than SATURN-MARS for the  $^{12}\text{C}(^{12}\text{C}, ^{13}\text{C})^{11}\text{C}_{\text{g.s.}}$  reaction at  $E/A = 50$  MeV, due to the modeling of the core-core interaction by PTOLEMY, which SATURN-MARS neglects.<sup>23</sup> For the proton-stripping reaction on the  $^{208}\text{Pb}$  target, where the Coulomb correction term in the interaction (also neglected in SATURN-MARS) is important, the PTOLEMY cross sections were about 10% lower than SATURN-MARS. In the latter case, the predictions of the two programs could be brought to agreement within a few percent<sup>24</sup> by adding a Coulomb correction term<sup>25</sup> to SATURN-MARS. The results presented below are those from PTOLEMY.

The Woods-Saxon potential used to generate the bound states for the mass-12 and mass-13 systems, and for  $^{27}\text{Al}+p$ , had a diffuseness of 0.65 fm, a reduced radius of 1.25 fm, and a spin-orbit potential strength of  $V_{\text{SO}} = 7$  MeV; similar parameters have been used in light-ion analyses of these systems.<sup>26,27</sup> For  $^{89}\text{Y}+p$  and  $^{40}\text{Ca}+n$ , the bound-state potential had a reduced radius of 1.20 fm and a diffuseness of 0.65 fm, as used in the analyses of Stuirbrink *et al.*<sup>16</sup> and Hansen *et al.*<sup>28</sup> For  $^{208}\text{Pb}+p$ , the bound-state potential shape was the same as used in Refs. 2 and 6; this shape fits the single-particle state energies of  $^{209}\text{Bi}$  best.<sup>2</sup>

##### B. Selection of optical-model potentials

Optical potentials for  $E/A = 50$ -MeV  $^{12}\text{C}$  elastic scattering are not currently available. Even if they were, there might still remain large uncertainties: Horen *et al.*<sup>29</sup> have shown that for heavy-ion reactions at high incident energies, different types of potentials that give similar elastic scattering cross sections can give rise to large differences in the probabilities for nucleon transfer

(see also Ref. 4). This happens if the partial-wave  $S$ -matrix elements for the potentials are very different in the region where the transfer radial integrals are most important. The potentials used in Ref. 29 had (i) a fairly deep real well (50 MeV), which gave reasonable cross sections, and (ii) a very shallow real well, which overpredicted the data at  $E/A = 20$  MeV by a factor of about 3.

On the other hand, the enhanced sensitivity at high energy of DWBA calculations in general to different OMP's means that elastic scattering data covering a wide angular range can select unambiguous heavy-ion potentials.<sup>30</sup> In particular, Brandan<sup>9</sup> has found a distinct preference for shallow-imaginary potentials with large radii and diffuseness in the fitting of  $^{12}\text{C}+^{12}\text{C}$  and  $^{12}\text{C}+^{16}\text{O}$  elastic scattering data that extend to very backward angles (For convenience, we will refer to this potential type as "shallow imaginary").

The potentials we have used here have come from various analyses of elastic scattering. Firstly, there is the rather extensive set of potentials found by Sahm *et al.*<sup>31</sup> from the analysis of  $E/A = 35$ -MeV  $^{12}\text{C}$  scattering on  $^{12}\text{C}$ ,  $^{40}\text{Ca}$ ,  $^{90}\text{Zr}$ , and  $^{208}\text{Pb}$ . These potentials all have deep-imaginary wells ( $\sim 200$  MeV) with either small radii or small diffuseness. We will refer to these potentials as "deep imaginary." Secondly, there are some shallow-imaginary potentials found from high-energy ( $E/A \approx 90$  MeV) heavy-ion scattering.<sup>32,33</sup> These potentials are similar to the ones found by Brandan,<sup>9</sup> and in fact a po-

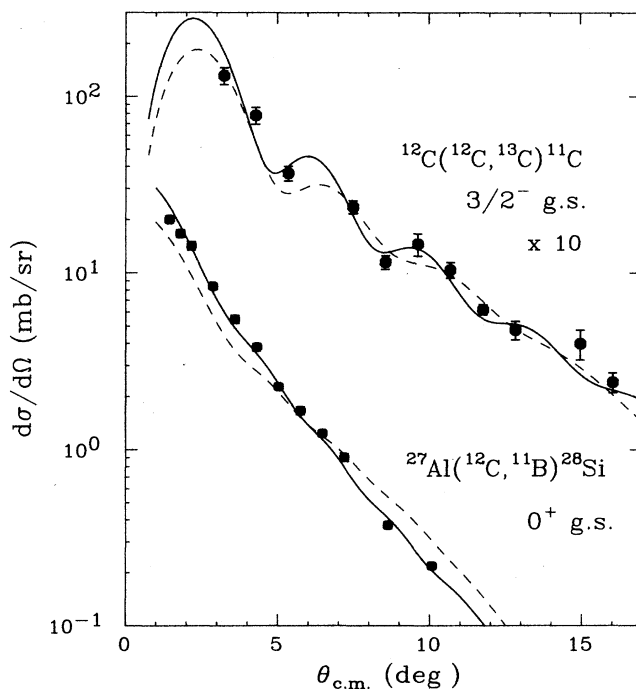


FIG. 3. Angular distributions for  $^{12}\text{C}(^{12}\text{C}, ^{13}\text{C})^{11}\text{C}$  (g.s.) and  $^{27}\text{Al}(^{12}\text{C}, ^{11}\text{B})^{28}\text{Si}$  (g.s.) at  $E/A = 50$  MeV. The curves are finite-range DWBA calculations, normalized to the data, with the following potentials.  $^{12}\text{C}$  target: C1 (solid line) and C2 (dashed line).  $^{27}\text{Al}$  target: CA1 (solid line) and SI3 (dashed line).

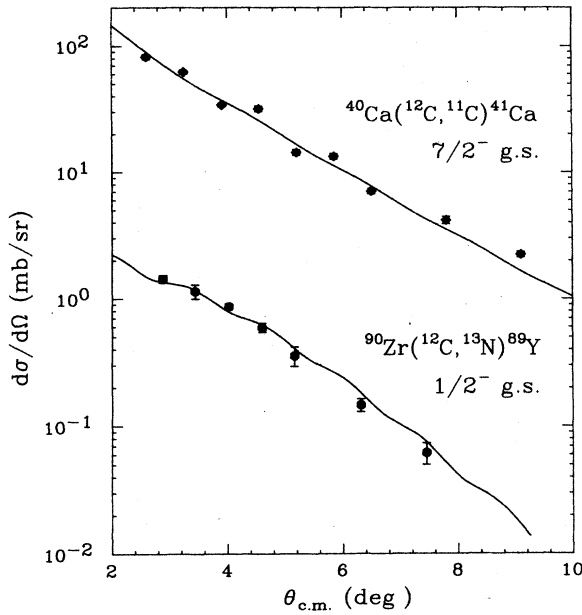


FIG. 4. Angular distributions for  $^{40}\text{Ca}(^{12}\text{C}, ^{11}\text{C})^{41}\text{Ca}$  (g.s.) and  $^{90}\text{Zr}(^{12}\text{C}, ^{13}\text{N})^{89}\text{Y}$  (g.s.) at  $E/A=50$  MeV. The curves are finite-range DWBA calculations, normalized to the data, with the optical-model potentials CA1 and ZR1, respectively.

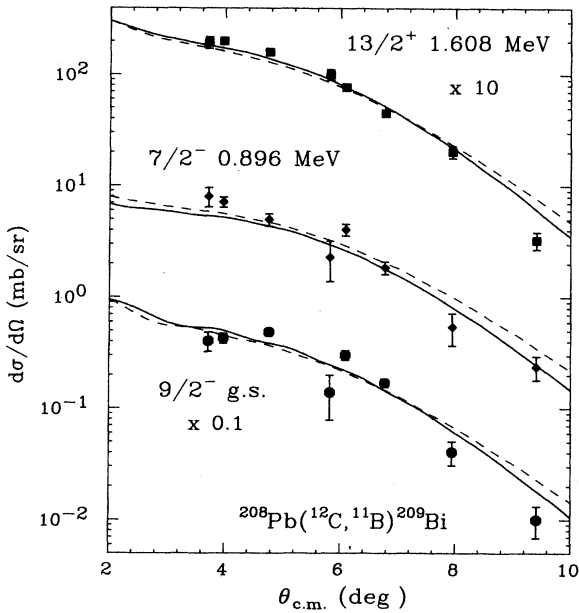


FIG. 5. Angular distributions for the one-proton stripping reaction  $^{208}\text{Pb}(^{12}\text{C}, ^{11}\text{B})^{209}\text{Bi}$  at  $E/A=50$  MeV. The curves are finite range DWBA calculations, normalized to the data, with the optical-model potentials PB4 (solid lines) and PB1 (dashed lines).

TABLE I. Target spectroscopic factors  $C^2S$  determined from the normalization of the DWBA predictions to the data. The column " $C^2S$  other" is a list of representative values from the literature.

Final state	$C^2S$	OMP	$C^2S$ other
$^{11}\text{C}$ g.s.	8.1	C1	3.0 <sup>a</sup>
	2.5	C2	
	2.3	Cx	
$^{28}\text{Si}$ g.s.	2.4	SI3	2.9 <sup>b</sup>
	7.7	CA1	
$^{41}\text{Ca}$ g.s.	0.83	CA1	0.89 <sup>c</sup>
$^{89}\text{Y}$ g.s.	2.2	ZR1	1.8 <sup>d</sup>
$^{209}\text{Bi}$ g.s.	0.20	PB4	0.68 <sup>e</sup> , 0.80 <sup>f</sup>
	0.49	PB1	
	0.90 MeV	PB4	0.94 <sup>e</sup> , 0.76 <sup>f</sup>
	0.60	PB1	
	1.61 MeV	PB4	
	0.45	PB1	1.00 <sup>e</sup> , 0.74 <sup>f</sup>

<sup>a</sup>Reference 26.

<sup>b</sup>Reference 27.

<sup>c</sup>Reference 28.

<sup>d</sup>Reference 16.

<sup>e</sup>Reference 6 with the OMP given here as PB4.

<sup>f</sup>Reference 34.

tential from Ref. 9 with the real depth interpolated for  $E/A=50$ -MeV scattering gives very similar results to the potential from Buenerd *et al.*<sup>32</sup> (see Sec. IV C). In addition to these, we have tried potentials from Ref. 6 for  $^{12}\text{C}+^{208}\text{Pb}$  scattering at  $E/A=40$  MeV. The same optical-model potentials were used in both entrance and exit channels for the transfer calculations presented here.

### C. Results

Angular distributions for all the extracted data are shown in Figs. 3–5. Only the angular distribution for the  $^{12}\text{C}$  target shows pronounced oscillations; the others display a rather smooth exponential falloff with angle. DWBA predictions, normalized to the data, also are shown in these figures.

The extracted target spectroscopic factors ( $C^2S$ ) are listed in Table I together with values obtained from other work (mostly light-ion reactions) for comparison. In order to obtain the target  $C^2S$ , the projectile spectroscopic factors have been taken as 3.0 for  $(^{12}\text{C}, ^{11}\text{C})$  and  $(^{12}\text{C}, ^{11}\text{B})$  and as 0.53 for  $(^{12}\text{C}, ^{13}\text{C})$  and  $(^{12}\text{C}, ^{13}\text{N})$ . These values represent average values from a compilation of experimental results for mass 11–13.<sup>26</sup>

The various optical-model potentials that were used in the DWBA calculations shown in Figs. 3–5 and that yielded the results presented in Table I are listed in Table II. For the  $^{12}\text{C}(^{12}\text{C}, ^{13}\text{C})^{11}\text{C}$  reaction, the  $E/A=35$ -MeV potential C1 from Sahn *et al.*<sup>31</sup> underestimates the section magnitude by more than a factor of 2. The  $E/A=85$ -MeV potential C2 from Ref. 32, which is of the shallow-imaginary type, gives much better agreement. Since the analysis of  $^{12}\text{C}+^{12}\text{C}$  elastic scattering by Bran-

TABLE II. Optical-model parameters of Woods-Saxon potentials used in the DWBA analyses. Potential depths are in MeV and geometrical parameters are in fm. The convention  $R = r(A_p^{1/3} + A_t^{1/3})$  is used.  $J_v/A$  and  $J_w/A$  are the real and imaginary volume integral per nucleon pair (in MeV fm<sup>3</sup>). The columns labeled "System" and " $E/A$ " refer to the elastic scattering from which the potential was obtained.

Label	$V$	$r$	$a$	$W$	$r_w$	$a_w$	$J_v/A$	$J_w/A$	Ref.	System	$E/A$
C1	250	0.814	0.626	231.9	0.789	0.60	481	405	31	<sup>12</sup> C + <sup>12</sup> C	35
C2	120	0.71	0.84	34.02	0.96	0.69	199	105	32	<sup>12</sup> C + <sup>12</sup> C	85
Cx	150	0.64	0.884	25.0	1.017	0.73	209	91	a	<sup>12</sup> C + <sup>12</sup> C	50
SI3	100	0.892	0.905	50.5	0.992	0.780	151	95	33	<sup>16</sup> O + <sup>28</sup> Si	94
CA1	200	0.870	0.75	281.1	0.869	0.678	262	355	31	<sup>12</sup> C + <sup>40</sup> Ca	35
ZR1	150	0.934	0.781	207.7	0.890	0.834	169	210	31	<sup>12</sup> C + <sup>90</sup> Zr	35
PB1	95	1.068	0.80	200.0	1.033	0.658	117	217	31	<sup>12</sup> C + <sup>208</sup> Pb	35
PB4	200	0.905	0.836	42.4	1.085	0.819	155	54	6	<sup>12</sup> C + <sup>208</sup> Pb	40
PB4b	50	1.082	0.792	50.0	1.082	0.792	64	64	6	<sup>12</sup> C + <sup>208</sup> Pb	40

<sup>a</sup>Parameters interpolated for  $E/A = 50$  MeV from the  $E/A = 30$  MeV and  $E/A = 85$  MeV potentials of Ref. 9.

dan<sup>9</sup> gave OMP's with rather smoothly varying parameters with incident energy, it was possible for us to extrapolate an  $E/A = 50$ -MeV potential. This is given in Table II as potential Cx. When used in a transfer calculation, both the shape of the angular distribution and the extracted value of  $C^2S$  were very similar to those with OMP C2.

For <sup>27</sup>Al(<sup>12</sup>C, <sup>11</sup>B)<sup>28</sup>Si, the shape of the angular distribution is reproduced somewhat better by the <sup>12</sup>C + <sup>40</sup>Ca OMP CA1 than the high-energy <sup>16</sup>O + <sup>28</sup>Si potential SI3 from Ref. 33, but the cross section again is underestimated by the lower-energy potential whereas the high-energy, shallow-imaginary-type potential gives a very reasonable  $C^2S$ .

On the other hand, the deep-imaginary potentials determined<sup>31</sup> at  $E/A = 35$  MeV appear to be quite adequate for the reactions on heavier mass targets (alternative choices of potentials given in Ref. 31 were tried and gave similar results). For the <sup>40</sup>Ca and <sup>90</sup>Zr targets, the Sahm *et al.* potentials CA1 and ZR1 give a good description of both the shape and magnitude of the angular distributions.

The potential PB4 determined by  $E/A = 40$  MeV from <sup>12</sup>C + <sup>208</sup>Pb by Mermaz *et al.*<sup>6</sup> overestimates the <sup>208</sup>Pb(<sup>12</sup>C, <sup>11</sup>B)<sup>209</sup>Bi cross section by a factor of approximately 3 (the OMP PB4b, also taken from Ref. 6, gave similar results). The OMP PB1 of Sahm *et al.*, despite having been determined at a lower energy, gives significantly better agreement with the data. The fact that the *relative* spectroscopic factors for the three states in <sup>209</sup>Bi agree quite well with those deduced from light ion work gives confidence in the peak-fitting procedure.

## V. CONCLUSIONS

The choice of an optical-model potential (OMP) for the generation of the distorted waves undoubtedly introduces the greatest uncertainty to the present analysis. It has been suggested<sup>35</sup> that angular distributions for high-energy transfer reactions might be able to discriminate against various OMP ambiguities if the angular range were large enough (see Fig. 6). While the angular range of the present data is too limited for such comparisons,

there is some evidence from the prediction of cross section *magnitudes* that shallow-imaginary potentials are more appropriate for the reactions on lighter targets. We also note that the potentials that yield reasonable values of  $C^2S$  generally have real volume integrals in the range 110–210 MeV fm<sup>3</sup> and imaginary volume integrals in the range 90–220 MeV fm<sup>3</sup> (see Table II). The volume integrals for potentials C1, PB4, and PB4b lie outside this apparent range of acceptability.

Our approach here has been to try various "reasonable" OMP's taken from the literature, the criteria for reasonableness being based on closeness to bombarding energy and projectile and target masses. Although the

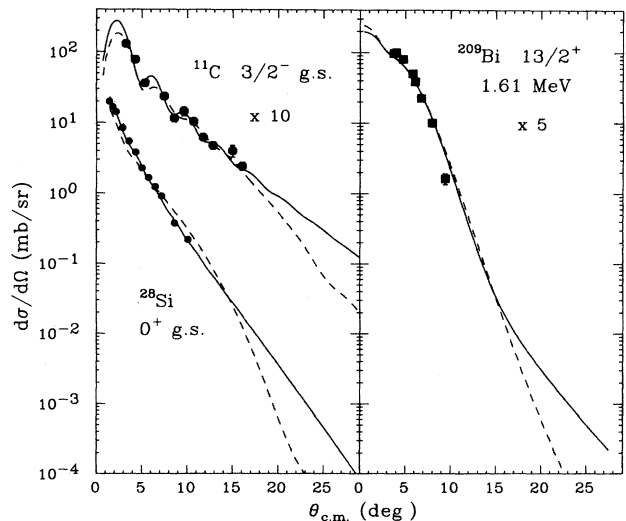


FIG. 6. Angular distributions plotted with an extended angular range to show the difference between the calculations at angles beyond  $\theta_{c.m.} \approx 15^\circ$  with either deep- or shallow-imaginary potentials. <sup>12</sup>C target: C1 (solid line) and C2 (dashed line). <sup>27</sup>Al target: CA1 (solid line) and SI3 (dashed line). <sup>208</sup>Pb target: PB4 (solid line) and PB1 (dashed line). (From a suggestion by Satchler and McVoy in Ref. 35.)

extracted spectroscopic factors have differed by up to a factor of 3 in the worst cases (see Table I), we have been able to show that there are some OMP's that give a satisfactory prediction of the cross-section magnitude. For the  $^{12}\text{C}$ ,  $^{27}\text{Al}$ ,  $^{40}\text{Ca}$ , and  $^{90}\text{Zr}$  targets the agreement with the data for the best cases is within 25%; for  $^{208}\text{Pb}$  the agreement with the OMP PB1 is not quite so good (about 50%). This may be contrasted with the  $^{16}\text{O}+^{208}\text{Pb}$  transfer reactions at  $E/A = 50$  MeV,<sup>2</sup> where there was a factor of 10 overprediction of the experimental cross section by the DWBA calculations, despite extensive trials of different OMP's. Note that for two of the cases in Table I, where the spectroscopic factors differ significantly with the light-ion results ( $^{11}\text{C}_{\text{g.s.}}$  with OMP C1, and  $^{28}\text{Si}_{\text{g.s.}}$  with OMP CA1), the DWBA calculations apparently *underpredict* the data.

The anomaly in the  $^{16}\text{O}+^{208}\text{Pb}$  stripping reactions at

high-energy thus appears to be specific to the  $^{16}\text{O}$  projectile. This suggests that the problem might be further investigated by studying transfer reactions induced by high-energy  $^{16}\text{O}$  or heavier projectiles on a wide mass range of targets.

#### ACKNOWLEDGMENTS

We would like to thank M. C. Mermaz and G. R. Satchler for useful discussions and for updated DWBA programs. We also acknowledge helpful communications from K. W. McVoy. This work was supported in part by the U. S. National Science Foundation under Grant Nos. PHY86-11210 [National Superconducting Cyclotron Laboratory (NSCL)] and PHY86-08227 (University of Michigan-Dearborn), and by the Academy of Athens (V. Notara Bequest).

\*Present address: Demokritos N.R.C., 15310 Ag. Paraskevi, P.O. Box 60228, Greece.

†Present address: Department of Health Physics, University of Michigan, Ann Arbor, MI 48109.

‡Presently also at National Superconducting Cyclotron Laboratory, Michigan State University, East Lansing, MI 48824.

<sup>1</sup>R. M. DeVries and J. C. Peng, Phys. Rev. C **22**, 1055 (1980).

<sup>2</sup>B. Berthier *et al.*, Phys. Lett. B **182**, 15 (1986); M. C. Mermaz *et al.*, Z. Phys. A **326**, 353 (1987).

<sup>3</sup>C. Olmer, M. C. Mermaz, M. Buenerd, C. K. Gelbke, D. L. Hendrie, J. Mahoney, D. K. Scott, M. H. Macfarlane, and S. S. Pieper, Phys. Rev. C **18**, 205 (1978); S. C. Pieper *et al.*, *ibid.* **18**, 180 (1978).

<sup>4</sup>M. A. G. Fernandes *et al.*, Phys. Rev. C **33**, 1971 (1986).

<sup>5</sup>W. von Oertzen, E. Adamides, M. Buenerd, J. Chauvin, D. Lebrun, J. Y. Hostachy, Ph. Martin, G. Perrin, and P. De Saintignon, Nucl. Phys. A **487**, 195 (1988).

<sup>6</sup>M. C. Mermaz *et al.*, Phys. Rev. C **37**, 1942 (1988); E. Tomasi-Gustafsson, These, de 3ème cycle, Université Paris-Sud (1988).

<sup>7</sup>J. S. Winfield, S. M. Austin, G. M. Crawley, C. Djalali, C. A. Ogilvie, R. J. Smith, Z. Chen, and M. Torres, Phys. Lett. B **203**, 345 (1988).

<sup>8</sup>J. Barrette, J. Phys. (Paris) **47**, C4 141 (1986).

<sup>9</sup>M. E. Brandan, Phys. Rev. Lett. **60**, 784 (1988).

<sup>10</sup>M. E. Brandan, S. H. Fricke, and K. W. McVoy, Phys. Rev. C **38**, 673 (1988); S. H. Fricke, M. E. Brandan, and K. W. McVoy, *ibid.* **38**, 682 (1988).

<sup>11</sup>B. M. Sherrill, Ph.D. thesis, Michigan State University (1983).

<sup>12</sup>D. M. Brink, Phys. Lett. **40B**, 37 (1972); W. von Oertzen, Phys. Lett. **151B**, 95 (1985).

<sup>13</sup>G. Ciangaru, C. C. Chang, J. R. Wu, R. W. Koontz, and H. D. Holmgren, Phys. Rev. C **29**, 2017 (1984).

<sup>14</sup>F. Videbaek, O. Hansen, B. S. Nilsson, E. R. Flynn, and J. C. Peng, Nucl. Phys. A **433**, 441 (1985).

<sup>15</sup>K. K. Seth, J. Picard, and G. R. Satchler, Nucl. Phys. A **140**, 577 (1970).

<sup>16</sup>A. Stuirbrink, G. J. Wagner, K. T. Knopfle, Lui Ken Pao, G. Mairle, H. Riedesel, K. Schindler, V. Bechtold, and L. Friedrich, Z. Phys. A **297**, 307 (1980).

<sup>17</sup>E. Adamides, H. G. Bohlen, W. von Oertzen, M. Buenerd, J. Chauvin, D. Lebrun, J. Y. Hostachy, Ph. Martin, G. Perrin, and P. De Saintignon, Nucl. Phys. A **475**, 598 (1987).

<sup>18</sup>R. Wadsworth, M. D. Cohler, M. J. Smithson, D. L. Watson, F. Jundt, L. Kraus, I. Linck, and J. C. Sens, J. Phys. G **9**,

1237 (1983).

<sup>19</sup>M. J. Martin, Nucl. Data **22**, 545 (1977).

<sup>20</sup>J. S. Larsen, J. L. C. Ford, Jr., R. M. Gaedke, K. S. Toth, J. B. Ball, and R. L. Hahn, Phys. Lett. **42B**, 205 (1972).

<sup>21</sup>M. H. Macfarlane and S. C. Pieper, Argonne National Laboratory Report No. ANL-76-11, 1976.

<sup>22</sup>T. Tamura and K. S. Low, Comput. Phys. Commun. **8**, 349 (1974).

<sup>23</sup>The core-core correction term was not included in the calculations done in Ref. 7. Because we normalized to the data, and shape changes were not large, this omission does not significantly affect the experimental values of  $\sigma_{\text{tot}}$  deduced in Ref. 7 with the aid of these calculations. However, the values of  $C^2S$  are affected. Calculations have been repeated with PTOLEMY, and the amended values for the product of the target and projectile spectroscopic factors are 2.5 at  $E/A = 25$  MeV (original value 2.2) and 2.45 at  $E/A = 35$  MeV (original value 1.95). The effect of the core-core correction on the cross-section magnitude appears to increase with increasing bombarding energy.

<sup>24</sup>M. C. Mermaz (private communication).

<sup>25</sup>J. C. Peng (unpublished).

<sup>26</sup>F. Ajzenberg-Selove, Nucl. Phys. A **433**, 1 (1985); A **449**, 1 (1986).

<sup>27</sup>J. Kalifa, G. Rotbard, M. Vergnes, and G. Ronsin, J. Phys. (Paris) **34**, 139 (1973).

<sup>28</sup>O. Hansen, J. R. Lien, O. Nathan, A. Sperduto, and P. O. Tjøm, Nucl. Phys. A **243**, 100 (1975).

<sup>29</sup>D. J. Horen, M. A. G. Fernandes, G. R. Satchler, B. L. Burks, R. L. Auble, F. E. Bertrand, E. E. Gross, D. C. Hensley, R. O. Sayer, and D. Shapira, Z. Phys. A **328**, 189 (1987).

<sup>30</sup>A. Nadasen *et al.*, Phys. Rev. C **37**, 132 (1988).

<sup>31</sup>C.-C. Sahn, T. Murakami, J. G. Cramer, A. J. Lazzarini, D. D. Leach, D. R. Tieger, R. A. Loveman, W. G. Lynch, M. B. Tsang, and J. van der Plicht, Phys. Rev. C **34**, 2165 (1986).

<sup>32</sup>M. Buenerd, A. Lounis, J. Chauvin, D. LeBrun, P. Martin, G. Duhamel, J. C. Gondrand, and P. de Saintignon, Nucl. Phys. A **424**, 313 (1984).

<sup>33</sup>P. Roussel, N. Alamanos, F. Auger, J. Barrette, B. Berthier, B. Fernandez, L. Papineau, H. Doubre, and W. Mittig, Nucl. Phys. A **477**, 345 (1988).

<sup>34</sup>S. Gales, C. P. Massolo, S. Fortier, J. P. Schapira, P. Martin, and V. Comparat, Phys. Rev. C **31**, 94 (1985).

<sup>35</sup>G. R. Satchler and K. W. McVoy (private communication).